Spectroscopic characterization by up conversion of Ho3+/Yb3+ codoped CdF2 single crystal

Sabrina Bordj, Hamid Satha, Anthony Barros, Daniel Zambon, Jean-Pierre Jouart, Madjid Diaf, Rachid Mahiou

Version of Record: https://www.sciencedirect.com/science/article/pii/S092534672100450X
Manuscript_7d6655a1308bd189dba70c539b86cd80

Spectroscopic Characterization by Up conversion of Ho^{3+}/Yb^{3+} codoped CdF_2 Single Crystal

Sabrina Bordj[a], Hamid Satha[b], Anthony Barros[c], Daniel Zambon[c], Jean-Pierre Jouart[d], Madjid Diaf[a], Rachid Mahiou[c,*]

[a] Laboratory of Laser Physics, Optical Spectroscopy and Optoelectronics (LAPLASO), Badji Mokhtar Annaba University, POB 12, 23000 Annaba, Algeria
[b] Laboratoire des Silicates, Polymères et des Nanocomposites, Université 8 mai 1945, Guelma, Algeria.
[c] Université Clermont Auvergne, CNRS, SIGMA Clermont, Institut de Chimie de Clermont-Ferrand, F-63000 Clermont-Ferrand, France
[d] ECATHERM/GRESPI, Reims Champagne-Ardenne University, France

*Corresponding author: rachid.mahiou@uca.fr

Abstract

Single crystal of CdF_2 codoped with the couple Ho^{3+}/Yb^{3+} with good optical quality were grown by a Bridgman technique after purification of the starting materials. Emission spectra are recorded at room temperature under UV and NIR excitation. The kinetics of the green and red emissions arising from both ($^5F_4$, $^5S_2$) and $^5F_5$ excited states of Ho^{3+} ions are analyzed in the frame of $Ho^{3+} \rightarrow Ho^{3+}$ and $Yb^{3+} \leftrightarrow Ho^{3+}$ energy transfers. The luminescence decays are parametrized using Inokuti-Hirayama model considering dipole-dipole interaction, in the case of UV excitation and also NIR excitation for the green emission, leading to a R_0 critical transfer distance of 9-11 Å. The kinetics of the $^5F_5 \rightarrow {}^5I_8$ red upconverted emission is analyzed and discussed using a rate equation model.

Keywords: cadmium fluoride, holmium and ytterbium, upconversion, kinetics, Inokuti-Hirayama, rate equation model

1. Introduction

In recent years visible and ultraviolet solid state lasers have attracted much attention due to the rapid growth of applications requiring tailored wavelength sources, such as full-color displays, optical data storage and biomedical instruments. Among various investigated systems, rare-earth-doped low phonon crystals or glasses have been reported as promising media for fiber and planar optical amplifiers and lasers [**1**]. Among the several investigated crystals, fluorides of the elements of group 2 of the periodic table are widely used as laser host material. The rare earth ions are usually applied as activators (dopants) for these fluorides. CdF_2 belongs to fluorite family of MF_2 (M=Ca, Sr, Ba, Pb, Hg^{2+}). The distinction of Cd belongs to the other M ions is the increase in nucleus charge comparatively to Sr by ten units, which gives rise to contraction of atom core. As result, the ionic size of Cd^{2+} is much less than that of Sr^{2+}. CdF_2 crystal can accommodate easily all trivalent rare-earth ions [**2**]. The substitutional RE^{3+} ions replace Cd^{2+} ions and the charge compensation is achieved at some distance by interstitial F_i^- ions. The presence of these ions increases the symmetry of the crystal field at the substituted trivalent ion site, making it remains mainly cubic in CdF_2. In addition, the Raman spectrum of CdF_2 crystal at room temperature consists of a strong depolarized line peaking at 315 cm^{-1} [**3**].
Using the energy upconversion (UC) phenomenon from rare earth ions is an effective approach to obtain visible laser under IR pumping. UC luminescence materials have also received special attention because of their prospective use in solar NIR concentrators for photovoltaic exploitation, IR sensing and biological labelling [**4, 5**]. In several UC processes Yb^{3+} ion is chosen as a sensitizer because of its simple two level energy structure and its high absorption cross-section at 980 nm which matches with the commercially available high power diode lasers along with its effective energy transfer capability to codoped activator ions. On the other hand Ho^{3+} ions have very distinct characteristic emission transitions both in the visible and IR wavelength range [**6**]. Yb^{3+} ion is used as sensitizer to augment the UC process since absorption cross-section of Yb^{3+} for NIR radiation is much higher than Ho^{3+}. The synthesis and spectroscopic properties of CdF_2 codoped Ho^{3+}/Yb^{3+} has already been reported [**7**]. However, the UC in this system was never reported. This is the subject of the present report where the emission of the Ho^{3+} ions *via* an NIR excitation provided by commercial 980 nm diode or by OPO pulsed laser for checking the dynamical processes ions and also in the UV wavelength range for comparison.

2. Sample properties and preparation

Cadmium difluoride (CdF_2) compound crystallizes in a face centered cubic structure, having the fluorite type and belonging to *Fm*3*m* (225) space group with four unit formula and cell parameter of 5.3810 Å. The crystallographic sites are Cd^{2+} (4a) and F^- (8c) with C_{4v} site symmetry for Cd^{2+} [**8-10**]. The ionic radius of Ho^{3+}, Yb^{3+} and Cd^{2+} is 89.4 pm, 85.8 pm and 95 pm, respectively. The crystal structure of CdF_2 is reported in Fig.1.
The CdF_2 single crystals are grown by use of the Bridgman technique from a vacuum furnace in fluorine atmosphere. The CdF_2 commercial powder, coming from Merck, is purified by repeated growth of simple crystals. After the purification step, the holmium and ytterbium doping ions are introduced in the form of trifluoride powders, HoF_3 and YbF_3, with nominal concentration of 1% for both ion ones. The mixture is heated under vacuum for 2 h with progressive temperature increase until 400 °C. The pulled crystal has more than 8 mm in diameter and 10–25 mm in length. Checked in polarized light, it is exempt of makles and crackles. It could easily cut into laser bulk single crystal with high optical quality. The sample

used for optical measurements was cut and polished to flat and parallel faces with 4.81 mm thickness (see inset of Fig.1).

3. Experimental procedure

All the measurements were carried out at room temperature.
Luminescence emission spectra and decays were recorded using a pulsed Nd:YAG OPO Ekspla NT342A laser (210-2600 nm, 3–5 ns pulse duration, 10 Hz, 5 cm^{-1} line width, 0.3 mJ-20 mJ in the UV and NIR range). The emitted photons were detected at right angle to the excitation and analyzed *via* an Edinburgh FLS980 spectrometer (Czerny-Turner monochromator, 300 mm focal length, 1200 grooves mm^{-1} grating and minimum pass band of 0.1 nm) equipped with Hamamatsu R928P PMT (200–850 nm range). The CW-NIR excitation is provided by a 980 nm beam of CW- diode laser CNI Model FC-980nm-4W. The UC emitted photons by the crystal are detected at right angle from the excitation and analyzed through a Horiba/Jobin-Yvon monochromator (Triax 550) combined with a cryogenically cold charge coupled device (CCD) camera (Horiba/Jobin-Yvon Symphony LN2 series).

4. Results and discussion

4.1: Steady state luminescence

4.1.1: Pulsed excitation

The recorded emission spectra under OPO pulsed laser at room temperature are reported in Fig.2, under excitation at 360 nm which corresponds to the $^5I_8 \rightarrow ^5G_4$ absorption transition of Ho^{3+} and in Fig.3, under excitation at 980 nm which is resonant within the $^2F_{7/2} \rightarrow ^2F_{5/2}$ absorption transition of Yb^{3+}.
The Stokes emission spectrum exhibits the emission bands peaking at 418, 486, 546, 580, 646 and 750 nm. On the basis of absorption spectrum reported in [**7**] and fluorescence spectra reported for $LaF_3:Ho^{3+}$ [**11**] and $CaF_2:Ho^{3+}$ [**12**] the five first emission bands correspond respectively to the transitions $^5G_5 \rightarrow ^5I_8$, $^5F_3 \rightarrow ^5I_8$, $(^5F_4, ^5S_2) \rightarrow ^5I_8$, $^5G_4 \rightarrow ^5I_6$, $^5F_5 \rightarrow ^5I_8$ (with possible overlap with the $^5F_3 \rightarrow ^5I_7$ [**12**]). The emission at 750 nm could be assigned to the $^5I_4 \rightarrow ^5I_8$ or to the $(^5F_4, ^5S_2) \rightarrow ^5I_7$ transitions or to the overlap of the two transitions, but the transition probability of the first one is very much smaller than that of the second [**13**]. On the other hand, the rise and decay of the luminescence at 750 nm, are similar with that measured for the time dependence of the 546 nm emission band (reported in the next section) which originates from the same $(^5F_4, ^5S_2)$ levels. This also supports the assignation of the 750 nm emission band to the $(^5F_4, ^5S_2) \rightarrow ^5I_7$ transitions. The UC emission spectrum exhibits mainly the $(^5F_4, ^5S_2) \rightarrow ^5I_8$, $^5F_5 \rightarrow ^5I_8$ and $(^5F_4, ^5S_2) \rightarrow ^5I_7$. However, the $^5F_3 \rightarrow ^5I_8$ emission is also recorded with very weak intensity as observed in the magnified part of the spectrum of Fig.3. For both spectra, the green emission related to the $(^5F_4, ^5S_2) \rightarrow ^5I_8$ transition is the most intense. The intensity ratio between green (546 nm) and red (646 nm) is ~ 3.8 under UV excitation and reaches ~ 13 under NIR pulsed excitation. Based on the above results, down conversion and up-conversion excitation and luminescence processes are proposed, as shown in Fig.4. The following mechanism is proposed for explaining the violet, blue, green and red emissions under excitation at 360 nm. Ho^{3+} absorbs UV photons to $^5G_4$ level, followed by nonradiative relaxations to $^5G_5$, $^5F_3$, $^5F_2$ and $^3K_8$ levels in turn *via* multiphonon relaxation. The $^5F_2$ state relaxes to the $^5F_3$ and $(^5F_4, ^5S_2)$ states in cascade, which emit the blue 486 nm $(^5F_3 \rightarrow ^5I_8)$ and green 546 nm $(^5F_4, ^5S_2 \rightarrow ^5I_8)$ radiations and also the red 750 nm $(^5F_4, ^5S_2 \rightarrow ^5I_7)$

emission. The partial population at $^5G_5$ level directly relax to $^5I_8$ states in cascade, which emit the violet 418 nm ($^5G_5 \rightarrow {}^5I_8$) radiation. The populations at ($^5F_4$, $^5S_2$) levels can be followed by nonradiative relaxation to $^5F_5$ state from which the 646 nm ($^5F_5 \rightarrow {}^5I_8$) red emission arises. The other possible channel for the feeding of the $^5F_5$ level is the resonant cross relaxation ($^5F_3 + {}^5I_8 \rightarrow {}^5F_5 + {}^5I_7$) as reported for YF_3: Ho^{3+} [**14**]. The band peaking at 580 nm is due to radiative relaxation for part of the population in $^5G_4$ to $^5I_6$. In the case of NIR excitation, as reported in several works, the ($^5F_4$, $^5S_2$) excited state is mainly populated *via* the ($^2F_{5/2}$, $^5I_6$) $\rightarrow$ ($^2F_{7/2}$, ($^5F_4$, $^5S_2$)) ETU process, followed by nonradiative relaxation to $^5F_5$ giving rise to green and red emissions at 546, 646 and 750 nm [**15**]. However, it seems that the mechanism responsible of for the Ho^{3+}:$^5F_5$ UC emission, as reported in $LiYF_4$:Ho^{3+} [**16**], involves only Ho^{3+} ions, with no Yb^{3+} contribution. An alternative mechanism for the $^5F_5$ UC luminescence involving only Ho^{3+} ions is outlined below. The weak blue emission at 486 nm ($^5F_3 \rightarrow {}^5I_8$) can also arise by two photon process, as observed in the case of $NaYF_4$:Yb^{3+}, Ho^{3+} [**15**], instead of four photon process. No emissions were observed from the upper $^5G_4$ and $^5G_5$, since in that case the UC process needs a simultaneous absorption of more than three NIR photons.

4.1.2: UC emission under CW excitation

In order to understand the UC mechanisms responsible for emerging the visible radiations, comparatively to pulsed excitation, a detailed discussion of the energy level diagram, as shown in Fig.4 has been considered. Fig.5 reports the measured (5a) and normalized (5b) emission spectra of CdF_2:1%Ho^{3+}, 1%Yb^{3+} under CW excitation at 980 nm. Only the visible green and red UC emissions, related to the $^5F_4$, $^5S_2 \rightarrow {}^5I_8$ and $^5F_5 \rightarrow {}^5I_8$ transitions of Ho^{3+}, are considered. However the intensity ratio I(546)/I(646) between the green ($^5F_4$, $^5S_2$) $\rightarrow$ $^5I_8$ transition and the red $^5F_5 \rightarrow {}^5I_8$ transition varies according to the pulsed and the CW excitation regimes, since on UC recorded spectra it reaches around ~ 4 and ~13 respectively. Moreover, this ratio is independent on the power pump of the NIR laser diode. Such difference indicates that the related dynamics between the green and red emission is different. Such difference will be discussed in the next section. In addition, usually, UC emission at 646 nm (red) occurs when the $^5F_5$ level is populated by non-radiative relaxation from the upper ($^5F_4 + {}^5S_2$) excited state after it relaxes radiatively to the $^5I_8$ ground state by emitting red photons. Thus, the decrease in the intensity of the red emission, at 980 nm excitation, is an indication that the non-radiative relaxation from the ($^5F_4 + {}^5S_2$) excited state to the lower $^5F_5$ level is weak. Another possibility is that a back transfer connecting the Ho^{3+}: $^5F_5$ level with the $^2F_{5/2}$ level of Yb^{3+} can occurs, leading to the decrease of the intensity arising from this level. This means that the $^5F_5$ level is more depopulated during two successive laser pulses than it's feeding from the de-excitation of the ($^5F_4$, $^5S_2$) levels.
In Fig.6, we have plotted the power dependence of the intensity of the green emission under a 980 nm excitation. The power of the diode is just an indication and is not corrected to provide the effective density in ions excited by cm^3. For an unsaturated up-conversion process, the number of photons which is responsible for the conversion mechanism can be calculated by [**17**]:

$$I_f \propto P^n \qquad (1)$$

where I_f is the fluorescent intensity, P is the pump power, and n is the number of the diode laser photons required. Double logarithmic plot of the relationship between pump energy and up-conversion emission integral intensities of the samples gives the slope n.
The log-log plot of the results leads to slope close to 2 which imply that a quadratic dependence indicating the mechanism involved is two photon UC processes as reported in

several papers related to the UC in Yb^{3+}-Ho^{3+} pairs embedded in glasses or crystals. Same result is obtained by considering the red emission peaking at 646 nm. Saturation is clearly observed when the power supply is fixed at value higher than ~ 260 mW/cm^2.

4.2: Luminescence decay analysis

Due to the limitation in emission detection of our experimental set-up, only the decays of Ho^{3+} in the visible range were recorded.
The decay of green emission, under UV excitation, is reported in Fig.7. It exhibits a rise time, as shown in the inset of this Fig.7, which corresponds to feeding of the ($^5F_4$, $^5S_2$) excited state from the upper levels ones. This rise time is followed by non-exponential decaying indicating that an energy transfer occurs from this level. In first approximation, the decay is fitted by simple sum of exponential functions, one in the rise and two in the tail of decay, leading to the time constants of 6.6 µs in the rise and 67 and 250 µs in the long decaying part (Table 1). The average lifetime in case of a bi-exponential decay can be calculated using the equation [**18**]:

$$\tau_{av} = \frac{A_1\tau_1^2 + A_2\tau_2^2}{A_1\tau_1 + A_2\tau_2} \qquad (2)$$

The derived τ_{av} from the fit is around ~ 202 µs (Table 1). All these values are lower than the estimated radiative lifetime reported for this excited state which is of 400 µs; value which is extracted from the analysis by Judd-Ofelt theory of the absorption spectrum of CdF_2:1% Ho^{3+}, 1%Yb^{3+} [**7**]. The reducing of the lifetime and exhibiting non-exponential shape is clearly an indication that energy transfer occurs, between the Ho^{3+} ions, or from Ho^{3+} ions to Yb^{3+} ions, also present in the host, as reported in the case of $CaSc_2O_4$: Ho^{3+},Yb^{3+} [**19**]. To understand the donor–acceptor interactions in the present host, well established theoretical model like 'Inokuti–Hirayama' (I-H) for direct energy transfer [**20**] can be used. Such fitting have been applied on the decay profiles of Ho^{3+} ions in the presence of acceptor, Ho^{3+} or Yb^{3+} ions by considering the ion interactions are dipole–dipole in nature due to the low concentration of active ions in the crystal CdF_2. When the energy transfer process is the cross-relaxation within a system of identical ions, the acceptor concentration equals the total concentration of activators.
In CdF_2 crystal, the concentration of active ions is of 2.55x10^{20} ions/cm^3 [**21**]**,** assuming the nominal doping level of 1% for both Ho^{3+} and Yb^{3+} , which becomes 5.10x10^{20} ions/cm^3 when we consider that both ions can act as acceptors, since an $Ho^{3+} \rightarrow Yb^{3+}$ energy transfer exits [**22, 23**]. This is due to the fact that in addition of radiative decay, Ho^{3+} ions in ($^5F_4$, $^5S_2$) level can also transfer their excitation energy to Yb^{3+} ions through the following cross-relaxation process:

$$Ho\ (^5F_4\ ,\ ^5S_2) + Yb\ (^2F_{7/2}) \rightarrow Ho\ (^5I_6) + Yb\ (^2F_{5/2}) \qquad (3)$$

For such purpose, the following equation where used to fit the decay of ($^5F_4$, $^5S_2$) $\rightarrow$ $^5I_8$:

$$I(t) = I_0 exp\left[-\frac{t}{\tau_0} - \frac{C_A}{C_0}\Gamma\left(1-\frac{3}{s}\right)\left(\frac{t}{\tau_0}\right)^{\frac{3}{s}}\right] \qquad (4)$$

where t=time; τ_0=lifetime for low acceptor ion concentration; s= 6, 8, or 10 for dipole–dipole, dipole–quadrupole, or quadrupole–quadrupole interactions, respectively; and Γ is Euler's gamma function : Γ(1-3/s) =1.77, 1.43, and 1.30 for s = 6, 8, and 10, respectively. C_A is the concentration of acceptor ions, and C_0 is the critical concentration given by C_0= 3 /(4πR_0^3) (R_0

is the critical transfer distance defined as that separation at which the rate of energy transfer between a donor–acceptor pair is equal to the intrinsic decay rate τ_0^{-1}). The donor–acceptor energy transfer parameter C_{DA} is related to R_0 as $C_{DA} = R_0^s x \tau_0^{-1}$. When we set s = 6 ($\Gamma(1-3/6) = 1.77$), and treat C_A/C_0 and τ_0 as adjustable parameters, the best fits of Eq. (4) to the experimental data are achieved (see Fig.7), which leads us to conclude that the interaction between Yb^{3+}/Ho^{3+} ions ($Ho^{3+} \rightarrow Ho^{3+} \rightarrow Yb^{3+}$) occurs *via* a dipole–dipole interaction. The derived and calculated values are gathered in Table 2.

However, the derived τ_0 value is 631 µs, value which is quite larger than that estimated in [**7**] (400 µs). Indeed, the use of the estimated τ_0 value leads to unsatisfactory fitting. Since we don't have a weakly doped crystal with Ho^{3+}, we can refer to the value of the radiative lifetime measured in CaF_2: 0.01% Ho^{3+} [**24**]. In this crystal, the green fluorescence related to the ($^5F_4$, $^5S_2$) $\rightarrow$ $^5I_8$ emission of Ho^{3+}, at room temperature under pulsed excitation at 488 nm, is characterized by single exponential decay with time constant of 666 µs. This value is close to that we have derived from our fitting (631 µs), confirming that the use of I-H model reproduces well the luminescence decay mechanism of the green emission. Then, the results of the fits show clearly that the luminescence dynamics process is more related to direct energy transfer than energy migration followed by transfer to acceptor.

In Fig.8, we have reported the decay of the red emission peaking at 646 nm, under UV excitation at 360 nm, arising from the $^5F_5$ excited level of Ho^{3+} ions. The decay exhibits no rise time indicating fast feeding of this level under UV excitation. The time constants derived using bi-exponential fitting are of ~ 47 and ~ 103 µs (Table 1), values which are largely shorter than that reported for the green emission peaking at 546 nm (67 and 250 µs with τ_{av} =202 µs, Table 1). The obtained τ_{av} using Eq.2 is of ~ 85 µs. It is not so far from that measured in $LiYF_4$:2% Ho^{3+}, 2% Yb^{3+} where it reaches ~102 µs [**16**]. As in the case of the green emission, the decay was also fitted using I-H model. The derived and calculated values leading to the best fit are gathered in Table 1. The value of τ_0 which leads to this best fit is 125 µs. This value of pure radiative lifetime of the $^5F_5$ excited level is largely lower than that derived from J-O analysis of absorption spectra in several fluorides, crystals of glasses which is between 1.2 ms and 400 µs. Notably this value is estimated as ~ 549 µs in CdF_2:1% Ho^{3+}, 1% Yb^{3+} [**7**]. Only few reports exist in the literature giving the direct measurement of this radiative lifetime, notably in weakly doped sample containing Ho^{3+} ions. The only value which is close to our derived estimation for this radiative lifetime is found for α-$NaYF_4$: Ho^{3+}, Yb^{3+} [**25**] in which the decay of the $^5F_5 \rightarrow ^5I_8$ emission at room temperature is fitted by a single exponential in the singly doped α-$NaYF_4$: 0.5% Ho^{3+} with time constant of 117 µs, value which is close to our derived τ_0 radiative time constant of the $^5F_5$ excited level (125 µs). To prove that our fit is consistent with the experimental results, we need to grow singly doped Ho^{3+} crystal with very low concentration, less than 1%. However, comparing the values derived from the fits by I-H for both green and red emissions, we observe that the C_{DA} (energy transfer microparameter) and R_0 critical transfer distance are quite always the same, around ~10^{-39} cm^6s^{-1} and ~9 Å and in the same order to that found in $LiYF_4$:Ho^{3+} [**26**] (1.2 x10^{-38} cm^6/s and 14.2 Å for d-d interaction respectively) and in several crystals or glasses activated by Ho^{3+} or Ho^{3+}-Yb^{3+} ion pairs [**27**]. This means that this value is a characteristic parameter which can be considered in the design of Ho^{3+}-Yb^{3+} pairs activated luminescent materials (optimum average distance between the active ions).

Fig.9 reports the decay of the UC green emission under excitation at 980 nm. As in the case of UV excitation the decay, in the first approximation, is fitted by exponential function in the rise and by bi-exponential function in the tail of the decay. The derived parameters from the fit are of 8.4 µs in the rise and 97 and 296 µs in the tail of the decay, leading to a τ_{av} of ~ 219 µs using Eq.2 (Table 1). The rise time and τ_{av} are in the same order than that measured under

UV excitation, 6.6 µs versus 8.4 µs, and 202 µs versus 219 µs respectively. Such observations seems to indicate that the feeding of the ($^5F_4$, $^5S_2$) level is quite similar under the UV or NIR excitations. Under UV excitation, the ($^5F_4$, $^5S_2$) level is filled by the relaxation from the upper states mainly $^5G_5$, $^5F_3$, levels from which an emission is observed as depicted in Fig.2. The feeding of the ($^5F_4$, $^5S_2$) level under NIR excitation needs in the first step a ground state absorption (GSA) in the Yb^{3+} ions followed by an $Yb^{3+} \rightarrow Ho^{3+}$ energy transfer which promotes the Ho^{3+} from their ground state $^5I_8$ to the phonon excited side states of the $^5I_6$ excited level from which, an excited state absorption (ESA) occurs by the absorption of second photon provided by the de-excitation of Yb^{3+} ions. After the two step excitation, inside of the Ho^{3+} ions (cooperative sensitization mediated by the $Yb^{3+} \rightarrow Ho^{3+}$ energy transfer), the ($^5F_4$, $^5S_2$) level is filled. This means that in that case, the rise time reflects more probably the decay time of the $^5I_6$ level which acts as reservoir for the second step and also perhaps that of the $^2F_{5/2}$ level of Yb^{3+} ions and that of the $^5F_3$ level, since 2 x $^2F_{5/2}$ (Yb^{3+}) $\rightarrow$ $^5F_3$ (Ho^{3+}) $\rightarrow$ ($^5F_4$, $^5S_2$) (Ho^{3+}) leads to the observation of the emission arising from the $^5F_3$, however with very weak intensity as observed on Fig.3. Nevertheless, the intrinsic radiative lifetime of the Yb^{3+}: $^2F_{5/2}$ level is expected to be long, as reported in the case of $Ca_{1-x}Yb_xF_{2+x}$, in which the measured value at x=0.2 is ~3 ms [**28**]. In addition, the derived absorption strength of the $^5I_8 \rightarrow ^5I_6$ transition of Ho^{3+} from absorption spectra of $CdF_2:Ho^{3+}$ is of ~ 9.2 x 10^{-20} cm^{-2} [**7**] which is high and comparable to that of the $^2F_{7/2} \rightarrow ^2F_{5/2}$ transition of Yb^{3+}, measured around ~ 1.9 x 10^{-20} cm^2 [**29**]. Such considerations lead to suppose that the observed build-up on the decay of the green emission is more probably related to feeding from the $^5I_6$ metastable level by ETU process through the ($^2F_{5/2}$, $^5I_6$) $\rightarrow$ ($^2F_{7/2}$, $^5S_2$/$^5F_4$), as suggested in [**16**] for $LiYF_4:Yb^{3+}$, Ho^{3+}, in addition of that from the $^5F_3$, which can perhaps explain why the rise is quite the same under both UV and NIR excitations.

On the same Fig.9, we have reported the fitting of the UC green emission using I-H model. In this case, we have considered that only the Ho^{3+} ions acts as acceptors, considering that $Ho^{3+} \rightarrow Yb^{3+}$ energy back transfer is expected to be weak. The derived and calculated parameters from the fit are reported in Table 2. As in the case of UV excitation, satisfactory fit is obtained using τ_0 value of 631 µs, derived from the UV excited green emission using I-H model, with reliability factor of 98.7%. This factor is notably enhanced when we use 590 µs as the τ_0 value, since this reliability factor reaches 99.8%. The two values of τ_0 lie in the same numerical range. In addition, the calculated R_0 critical transfer distance (~ 11 Å) is similar to that found under UV excitation, in agreement with our assessment that the decaying dynamics from the ($^5F_4$, $^5S_2$) excited level is independent on the excitation used, UV or NIR.

Fig.10 shows the luminescence decay of the red emission ($^5F_5 \rightarrow ^5I_8$) under NIR excitation at 980 nm. The experimental points are largely dispersed due to the weak luminescence intensity recorded under our setup with pulsed excitation laser. The decay consists of rise time followed by exponential decaying. The time constants derived from the fit are of 15 µs in the rise and 43 µs in the tail. These values diverge notably from that reported under NIR excitations in $LiYF_4$:0.5% Ho^{3+}, (27 µs and 105 µs respectively under excitation at 890 nm into the $^5I_5$ level) [**30**] and in $LiYF_4$:2% Yb^{3+}, 20% Ho^{3+} (20 µs and 770 µs respectively under excitation at 1150 nm into the $^5I_6$ level) [**16**], while for such compounds, direct excitation of the $^5F_5$ level lead to decays times of 105 µs [**30**] and 102 µs [**16**]. Surprisingly, its appears from these two works [**16, 30**] that the rise time of the UC red emission is quite similar despite that the lifetimes of the $^5I_6$ and $^5I_5$ excited states are notably different: 1.6 ms [**12, 16**] and 20 µs [**12, 30**] respectively. The situation is then different than that of the green emission for which the decays are quite similar under both UV and NIR excitations. Under UV excitation, the feeding of the $^5I_6$ level is provided by de-excitation from upper excited states, such as $^5G_4$, $^5F_3$, $^5F_5$, ($^5F_4$, $^5S_2$) [**12**]. Under NIR excitation, the Ho^{3+} ions are promoted in this

excited state by direct energy transfer from Yb^{3+} ions. Part of these Ho^{3+} ions in their $^5I_6$ excited state become not available for their feeding by the de-excitation from the upper levels. Such assumption is supported by the increase of τ_{av} of the green emission under NIR excitation (Table 1) since the non-radiative rate of this emission is decreased. Another consequence of the direct feeding of the $^5I_6$ level is the increase the cross-relaxation (CR) connecting the $^5F_5$ and $^5I_6$ levels ($^5F_5$, $^5I_8 \rightarrow {}^5I_6$) which provides de-excitation channel, leading to the decrease of the intensity of the $^5F_5 \rightarrow {}^5I_8$ emission under pulsed excitation since this CR is expected to be efficient occurring during low repetition-rate nanosecond pulse excitation (10 Hz, 5ns).

The shape of the decay of the red emission arising from the $^5F_5$ level under NIR excitation is clearly different from that recorded under UV excitation. Based on the luminescence processes proposed, as shown in Fig.4 and on the discussion made above; we can then consider that the UC process can be represented by a simple three level system where the intermediate state at the present stage can be $^5I_7$ or $^5I_6$ even the $^5I_5$ without further distinctions. The $^5I_7$ level is populated *via* cross relaxation from the $^5I_6$ level ($^5I_8$, $^5F_5 \rightarrow {}^5I_6$, $^5I_7$) more probably than by non-radiative relaxation from the $^5I_6$ [**12**] despite that this non-radiative relaxation seems to be not very efficient as suggested for $LiYF_4:Yb^{3+}$, Ho^{3+} [16]. Moreover two Ho^{3+} ions in the $^5I_6$ excited state can interact *via* the ($^5I_6$, $^5I_6$) $\rightarrow$ ($^5I_7$, $^5I_5$) leading to the population of the $^5I_5$ level. This means that mechanism of ion-ion interaction between Ho^{3+} ions is responsible for populating of $^5F_5$ level. The use of one of these levels as the intermediate state comes from the fact that the Log-Log plot of the red emission under CW-excitation versus the power of the NIR laser diode leads to quadratic dependence. In this simplified model (see inset of Fig.4), the time dependent populations of different energy states can be described by the following rate equations [**31**] valid in the case of ion-ion interaction between two identical ions [**32**]:

$$\frac{dN_1}{dt} = N_0 AI - W_1 N_1 - W_T N_1^2 \qquad (5)$$

$$\frac{dN_2}{dt} = \frac{1}{2} W_T N_1^2 - W_2 N_2 \qquad (6)$$

where N_0, N_1 and N_2 stand for the population densities of the ground state $^5I_8$ and excited states Is (Is for intermediate state) and $^5F_5$ respectively. W_1 and W_2 are the decaying rate of the Is and $^5F_5$ levels. AI is the product of the absorption cross-section with the laser intensity and W_T is ETU rate. The system of these two equations has no analytical solution and can be solved through numerical simulations as reported for example in [**33, 34**]. However, in the low pumping regime the term $W_T N_1^2$ can be neglected in Eq.5 [**32**]. In these conditions, the integrated intensities $I_1(t)$ and $I_2(t)$ are directly proportional to the populations

$$I_1(t) = I_1(0) e^{-W_1 t} \qquad (7)$$

$$I_2(t) = \frac{1}{2} \frac{W_T I_1^2(0)}{W_2 - 2W_1} (e^{-2W_1 t} - e^{-W_2 t}) \qquad (8)$$

Eq.8 refers to the up converted emission and can be rewritten using $W_1 = 1/\tau_1$ and $W_2 = 1/\tau_2$

$$I_2(t) \propto \frac{\tau_1\tau_2}{(\tau_1-2\tau_2)}\left(e^{-2t/\tau_1} - e^{-t/\tau_2}\right) \qquad (9)$$

were τ_1 and τ_2 stand for the values of the kinetics of both Is intermediate level, and $^5F_5$ emitting state, obtained under direct laser excitations in the singly Ho^{3+} doped material, neglecting a possible de-excitations, by energy transfer to unwanted acceptors, or by cross-relaxations . The rise is always attributed to the level which exhibits more fast decay [**32**]. On Fig.10, we have reported the fitting of the decay of the UCL from $^5F_5$ level under NIR excitation using Eq.9. The values derived from the best fit are of 15 µs in the rise and 43 µs in the tail as reported above (Table 1). We have no information about the decay times of the $^5I_7$ $^5I_6$ and $^5I_5$ levels in $CdF_2:Ho^{3+}$. If we consider that $\tau_1 > 2\tau_2$ Eq.9 leads to lifetime nearly the half of that for the considered state under Stokes excitation. It seems that this situation is fulfilled considering the $^5F_5$ level since the estimated lifetime is 85 µs (Table 1), ~ 100 µs in $LiYF_4$: Ho^{3+} [**30**] and $LiYF_4$: Yb^{3+}, Ho^{3+} [**16**] : 85 µs/2 ≃ 43 µs as measured from Fig.10. In this frame, the recorded rise time is puzzling, since only the $^5I_5$ level with lifetime of 20 µs can satisfy Eq.9. Such rise time value is reported for $LiYF_4$:0.5% as discussed above [**30**]. The $^5I_7$ and $^5I_6$ are metastable states with long effective lifetime of the order of several milliseconds. In the case of $LiYF_4$: 2% Ho^{3+}, 20% Yb^{3+} [**16**] the rise time measured for the UC red emission arising from the $^5F_5$ excited state (20 µs) is assumed to be related to the inverse of energy transfer rate through ($^5I_6$, $^5I_6$) → ($^5I_7$, $^5I_5$) energy transfer process (23 µs in the simulated decay). However, in this paper the time constant measured in the tail of the decay is of 770 µs (instead of 102 µs under direct excitation of the $^5F_5$ level), and can corresponds, perhaps to half of the lifetime of the $^5I_6$ level (770 µs ≃ 1.6 ms/2) assuming Eq.9. To provide support for the mechanism for the $^5F_5$ Ho^{3+} UC emission in CdF_2: 1%Yb^{3+}, 1% Ho^{3+}, several experiments must be performed, notably by recording the decays of the UC red emission under selective excitation in the $^5I_7$, $^5I_6$ and the $^5I_5$ levels.

5. Conclusion

We have studied down and upconversion luminescence mechanisms at room temperature in CdF_2:1% Ho^{3+}, 1% Yb^{3+} single crystal. OPO pulsed laser in addition to CW -980 nm-laser diode were used to investigate the emission and luminescence decays arising from the main excited stated of Ho^{3+}, namely ($^5F_4$, $^5S_2$) and $^5F_5$ levels. Several cross-relaxations connect the excited states of Ho^{3+} under both UV and NIR excitations in addition of upconversion energy transfer (ETU), ground state absorption (GSA) and excited state absorption (ESA) involving the feeding of the $^5I_6$ and $^5I_7$ excited states of Ho^{3+}. They have been used to propose a diagram depicting the several exciting/decaying channels for the green and red emissions. The upconversion mechanism is a two-photon process as usually reported for such Yb^{3+}/Ho^{3+} pair. The analyses of the kinetics are discussed considering that $Ho^{3+} \rightarrow Ho^{3+}$ and $Yb^{3+} \leftrightarrow Ho^{3+}$ energy transfer pathways exist in this system. The luminescence decays of the green ($^5F_4$, $^5S_2$)→$^5I_8$, and red $^5F_5$→$^5I_8$ are discussed. The green emission decays are characterized by same dynamics shapes suggesting that the ($^5F_4$, $^5S_2$) level is fed in rather similar way under either UV or NIR excitations. Such consideration is supported by the fact that the temporal decaying of this emission is well reproduced using I-H model, considering dipole-dipole electrical interaction between the active ions, leading to an R_0 critical transfer distance of 9-11 Å. The feeding of the $^5F_5$ depends on the excitation used. Under UV excitation, this excited

state presents no rise time indicating that its population is reached quickly, probably during the laser pulse duration, due to an effective fast cross relaxation or a non-radiative de-excitation from the ($^5F_4$, $^5S_2$) level. Under NIR excitation, the luminescence decay of the emission arising from the $^5F_5$ is parametrized using a rate equation system considering a simple three level system, where the intermediate level is not clearly attributed.

Acknowledgements

H.S. is grateful for the MESRS from Algeria for providing a grant in the frame of sabbatical year for scientific stay in France (Ref.: N° 082/CS/MESRS/DCEIU/2015). He is also grateful for the ICCF-UMR 6296 for the accessing to their facilities and for their supporting as visiting scientist during 2015-2016.

Author Contributions

The manuscript was written through contributions of all authors.

CRediT authorship contribution statement

S. Bordj: Investigation, Data curation. H. Satha: Supervision, Validation, Visualization, Project administration, Writing - review & editing. A. Barros: Formal analysis, Data curation, Visualization. D. Zambon: Formal analysis, Data curation, Visualization. J.P. Jouart: Methodology, Formal analysis. M. Diaf: Supervision, Validation, Visualization, Project administration, Writing - review & editing. R. Mahiou: Conceptualization, Supervision, Validation, Visualization, Project administration, Writing – original draft, Writing - review & editing, Funding acquisition.

Declaration of Competing Interest

The authors declare that they have no known competing financial interests or personal relationships that could have appeared to influence the work reported in this paper.

References

[**1**]. D.S. Funk , J.G. Eden, IEEE J. Sel. Top. Quantum Electron., Glass-fiber lasers in the ultraviolet and visible**,** 1(3) (1995) 784-791.
https:// doi.org/10.1109/2944.473660

[**2**] J-P. Jouart, C. Bissieux, M. Egee, G. Mary, M. de Murcia, Optical study of Eu^{3+} centres in CdF_2, J. Phys. C: Solid State Phys., 14 (1981) 4923-4935.
https://iopscience.iop.org/article/10.1088/0022-3719/14/32/025

[**3**] N. Krishnamurthy, V**.** Soots, Raman spectra of CdF_2 and PbF_2, Can. J. Phys., 48 (1970) 1104-1107.
https://doi.org/10.1139/p70-143

[**4**] A. Shalav, B.S. Richards, M.A. Green, Luminescent layers for enhanced silicon solar cell performance: Up-conversion**,** Sol. Energy Mater. Sol. Cells, 91 (2007) 829–842.
https://doi.org/10.1016/j.solmat.2007.02.007

[**5**] J-H. Zeng, J. Su, Z.-H. Li, R.-X. Yan, Y.-D. Li, Synthesis and Upconversion Luminescence of Hexagonal-Phase $NaYF_4$:Yb, Er^{3+} Phosphors of Controlled Size and Morphology, Adv. Mater., 17 (2005) 2119–2123.
https://doi.org/10.1002/adma.200402046

[**6**] M.J. Weber, B.H. Matsinger, V.L. Donlan, G.T. Surratt, Optical Transition Probabilities for Trivalent Holmium in LaF_3 and $YAlO_3$, J. Chem. Phys., 57 (1972) 562–567.
https://doi.org/10.1063/1.1678000

[**7**] R. Fartas, M. Diaf , H. Boubekri, L. Guerbous , J.P. Jouart, Synthesis and study of spectroscopic properties of CdF_2 crystals codoped with luminescent rare earth ions (Ho^{3+}/Yb^{3+}), J. Alloys. Comp., 606 (2014) 73–80.
http://dx.doi.org/10.1016/j.jallcom.2014.04.028

[**8**] E. Banks, P. Wagner, Effects of Charge Compensation on the Absorption Spectrum of Yb^{3+} in Cadmium Fluoride, J. Chem. Phys., 44 (1966) 713-717.
https://doi.org/10.1063/1.1726750

[**9**] R.W.G. Wyckoff, (1963), Crystal Structures (New York: Interscience)

[**10**] S.P. Ivanov, I.I. Buchinskaya, P.P. Fedorov, Distribution Coefficients of Impurities in Cadmium Fluoride, Inorg. Mater., 36 (2000) 392-396.
https://link.springer.com/article/10.1007/BF02758088

[**11**] H. H. Caspers, H. E. Rast, L. Fry, Absorption, Fluorescence, and Energy Levels of Ho^{3+} in LaF_3**,** J. Chem. Phys., 53, 3208 (1970) 3208-3216.
http://dx.doi.org/10.1063/1.1674471

[**12**] A.A. Lyapin, P.A. Ryabochkina, A.N. Chabushkin, S.N. Ushakov, P.P. Fedorov, Investigation of the mechanisms of upconversion luminescence in Ho^{3+} doped CaF_2 crystals and ceramics upon excitation of $^5I_7$ level, J. Lumines., 167 (2015) 120-125.
http://dx.doi.org/10.1016/j.jlumin.2015.06.011

[**13**] K. Tanimura, M. D. Shinn, W. A. Sibley, M. G. Drexhage, R. N. Brown, Optical transitions of Ho^{3+} ions in fluorozirconate glass, Phys. Rev. B, 30 (1984) 2429-2437.
https://doi.org/10.1103/PhysRevB.30.2429

[**14**] J.F. Pouradier, F.E. Auzel, Calcul des probabilités des transferts d'énergie entre ions de terres rares. II. Transferts $Ho^{3+} \rightarrow Ho^{3+}$ dans le fluorure mixte $Ho_xY_{1-x}F_3$, Journal de Physique, 39(8) (1978), 833-837.
http://dx.doi.org/10.1051/phys:01978003908083300

[**15**] A.Pilch, D.Wawrzyńczyk, M.Kurnatowska, B.Czaban, M.Samoć, W.Strek, A.Bednarkiewicz, The concentration dependent up-conversion luminescence of Ho^{3+} and Yb^{3+} co-doped β-$NaYF_4$, J. Lumines., 182 (2017) 114-122.
http://dx.doi.org/10.1016/j.jlumin.2016.10.016

[**16**] R. Martín-Rodríguez, A.Meijerink, Infrared to near-infrared and visible upconversion mechanisms in $LiYF_4$: Yb^{3+}, Ho^{3+}, J. Lumines., 147 (2014) 147–154.
http://dx.doi.org/10.1016/j.jlumin.2013.11.008

[17] M. Pollnau, D.R. Gamelin, S.R. Lüthi, H.U. Güdel, M.P. Hehlen, Power dependence of upconversion luminescence in lanthanide and transition-metal-ion systems, Phys. Rev. B, 61(2000) 3337–3346.
https://doi.org/10.1103/PhysRevB.61.3337

[18] J.W. Stouwdam, F.C.J.M. van Veggel, Near-infrared Emission of Redispersible Er^{3+}, Nd^{3+}, and Ho^{3+} Doped LaF_3 Nanoparticles, Nano Lett., 2 (2002) 733-737.
https://doi.org/10.1021/nl025562q

[19] S. Georgescu, A. Stefan, A-M. Voiculescu, O. Toma, C. Matei, R. Birjega, Peculiarities of the Ho^{3+}-Yb^{3+} energy transfer in $CaSc_2O_4$:Ho:Yb, J. Lumines., 154 (2014) 142–147.
http://dx.doi.org/10.1016/j.jlumin.2014.04.021

[20] M. Inokuti, F. Hirayama, Influence of energy transfer by the exchange mechanism on donor luminescence, J. Chem. Phys., 43 (1965) 1978–1989.
https://doi.org/ 10.1063/1.1697063

[21] E.A. Ryzhova, V.N. Molchanov, A.A. Artyukhov, V.I. Simonov, B.P. Sobolev, Growth and Defect Crystal Structure of CdF_2 and Nonstoichiometric $Cd_{1-x}R_xF_{2+x}$ Phases (R = Rare Earth Elements and In). 2. Methods of Structure Refinement of $Cd_{0.90}R_{0.10}F_{2.10}$ Phases Using the Example of $Cd_{0.90}Tb_{0.10}F_{2.10}$ Structure of Nanodimensional Clusters in $Cd_{0.90}Tb_{0.10}F_{2.10}$ Crystal, Crystallogr. Rep., 49 (2004) 668-675.
https://doi.org/1063-7745/04/4904

[22] J. Zhang, Y. Wang, L. Guo, P. Dong, Upconversion Luminescence and Near-infrared Quantum Cutting in $Y_6O_5F_8$:RE^{3+} (RE = Yb, Er, and Ho) with Controllable Morphologies by Hydrothermal Synthesis, Dalton Trans., 42 (2013) 3542-3451.
https://doi.org/10.1039/C2DT32463F

[23] X. X. Zhang, P. Hong, M. Bass, B.H.T. Chai, Ho^{3+} to Yb^{3+} back transfer and thermal quenching of upconversion green emission in fluoride crystals, Appl. Phys Lett., 63(19) (1993) 2606-2608.
https://doi.org/10.1063/1.110445

[24] B. Lal, D. Ramachandra Rao, Fluorescence and lifetime studies of Ho^{3+}: CaF_2, Chem. Phys. Lett., 53(2) (1978) 250-254.
https://doi.org/10.1016/0009-2614(78)85390-1

[25] K. Deng, T. Gong, L. Hu, X. Wei, Y. Chen, M. Yin, Efficient near-infrared quantum cutting in $NaYF_4$: Ho^{3+}, Yb^{3+} for solar photovoltaics, Opt. Express, 19(3) (2011) 1749-1754.
https://www.osapublishing.org/DirectPDFAccess/868FB26F-C0C5-4194-F35E9AAA3E3804D3_209551/

[26] L. Gomes, L. C. Courrol, L. V. G. Tarelho, I. M. Ranieri, Cross-relaxation process between +3 rare-earth ions in $LiYF_4$ crystals, Phys. Rev. B 54 (1996) 3825-3829.
https://doi.org/10.1103/PhysRevB.54.3825

[27] S. Balaji, A. K. Mandal, K. Annapurna, Energy transfer based NIR to visible upconversion: Enhanced red luminescence from Yb^{3+}/Ho^{3+} co-doped tellurite glass, Opt. Mater., 34 (2012) 1930-1934.

http://dx.doi.org/10.1016/j.optmat.2012.05.037

[28] M. Ito, C. Goutaudier, Y. Guyot, K. Lebbou, T. Fukuda, G. Boulon, Crystal growth, Yb^{3+} spectroscopy, concentration quenching analysis and potentiality of laser emission in $Ca_{1-x}Yb_xF_{2+x}$, J. Phys. Condens. Matter., 16 (2004) 1501–1521.
https://doi.org/10.1088/0953-8984/16/8/029.

[29] S. Balaji, G. Gupta, K. Biswas, D. Ghosh, K. Annapurna, Role of Yb^{3+} ions on enhanced ~2.9 μm emission from Ho^{3+} ions in low phonon oxide glass system**,** Scientific Reports | 6:29203 |.
http://dx.doi.org/10.1038/srep29203

[30] B.M. Walsh, Spectroscopy and Excitation Dynamics of the Trivalent Lanthanides Tm^{3+} and Ho^{3+} in $LiYF_4$, NASA-CR-4689 (1995), 73-75.
https://core.ac.uk/download/pdf/42779752.pdf

[31] R. Mahiou, B. Jacquier, C. Madej, One-dimensional energy transfer in $GdCl_3$, J. Chem. Phys., 89 (1988) 5931–5942.
https://doi.org/10.1063/1.455544

[32] D. Gamelin, H. Güdel, in Transition Metal and Rare Earth Compounds, ed. H. Yersin, Springer Berlin/Heidelberg, vol. 214 (2001) 1-56.

[33] J. Bergstrand, Q. Liu, B. Huang, X. Peng, C. Würth, U. Resch-Genger, Q. Zhan, J. Widengren, H. Ågren, H. Liu, On the decay time of upconversion luminescence, Nanoscale., 11 (2019) 4959–4969.
https://doi.org/10.1039/C8NR10332A

[34] J. Kong, X. Shang, W. Zheng, X. Chen, D. Tu, M. Wang, J. Song, J. Qu, Revisiting the Luminescence Decay Kinetics of Energy Transfer Upconversion, J. Phys. Chem. Lett., 11 (2020) 3672–3680.
https://doi.org/10.1021/acs.jpclett.0c00619.

Figure captions

Figure 1: Crystal structure of CdF_2. The inset shows cut and polished crystal sample

Figure 2: Emission spectrum of CdF_2:1%Ho^{3+}, 1%Yb^{3+} single crystal under pulsed excitation at 360 nm.

Figure 3: UC emission spectrum of CdF_2:1%Ho^{3+}, 1%Yb^{3+} single crystal under pulsed excitation at 980 nm. The added picture shows bright green UC emission corresponding to the main emission ($^5F_4$, $^5S_2$) $\rightarrow$ $^5I_8$ under 980 nm excitation.

Figure 4: Energy transition diagram of Yb^{3+}/Ho^{3+} ions in CdF_2:1%Ho^{3+}, 1%Yb^{3+} under UV (360 nm) and NIR (980 nm) excitations. ETU is related to the $Yb^{3+}\rightarrow$ Ho^{3+} energy transfer by upconversion, and B.T to the $Ho^{3+}\rightarrow$ Yb^{3+} energy back transfer. The inset shows the simple energy levels diagram used for the red UC emission.

Figure 5: Mesured (5a) and Normalized (5b) UC emission spectra of CdF_2:1%Ho^{3+}, 1%Yb^{3+} versus the power of the CW-980 nm laser diode.

Figure 6: Log of green UC emission at 546 nm versus the log power of the CW-980 nm laser diode. The solid line represents the linear fitting which leads to slope of 1.86.

Figure 7: Decay profile of green ($^5F_4$, $^5S_2$) $\rightarrow$ $^5I_8$ emission of Ho^{3+} ions under UV excitation at 360 nm. The red solid line represents the fitting obtained using bi-exponential decaying and the green solid line represents the fit obtained using I-H model as discussed in the text. The inset shows the fitting of the rise time recorded under UV excitation.

Figure 8: Decay profile of red $^5F_5\rightarrow$$^5I_8$ emission of Ho^{3+} ions under UV excitation at 360 nm. The red solid line represents the fitting obtained using bi-exponential decaying and the green solid line represents the fit obtained using I-H model as discussed in the text.

Figure 9: Decay profile of green ($^5F_4$, $^5S_2$) $\rightarrow$ $^5I_8$ emission of Ho^{3+} ions under NIR excitation at 980 nm. The red solid line represents the fitting obtained using bi-exponential decaying and the green solid line represents the fit obtained using I-H model as discussed in the text. The inset shows the fitting of the rise time recorded under NIR excitation.

Figure 10: Decay profile of red $^5F_5\rightarrow$$^5I_8$ emission of Ho^{3+} ions under NIR excitation at 980 nm. The solid line represents the fitting obtained using bi-exponential decaying (one in the rise and another in the tail of the decay) derived from the rate equation model as discussed in the text.

Figure 1

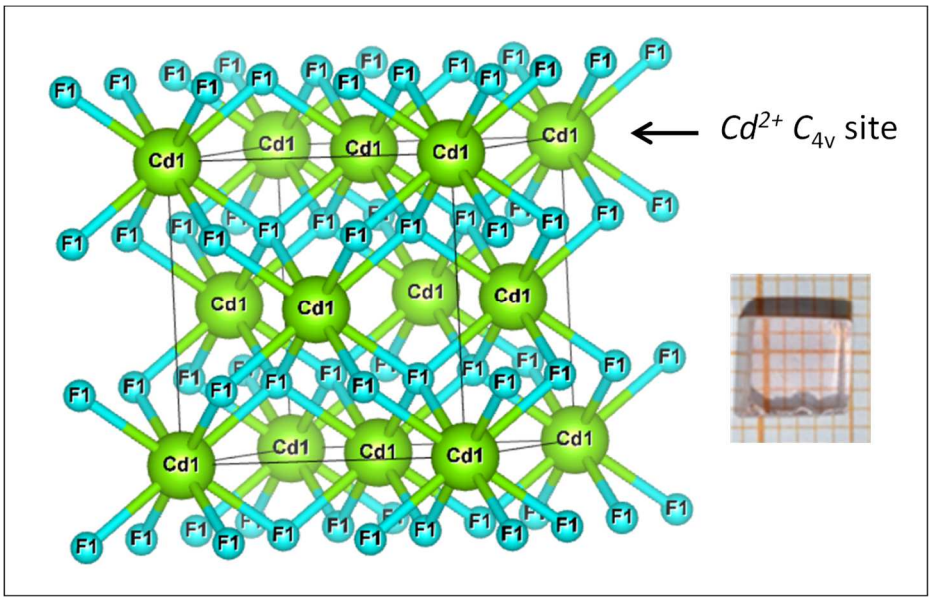

Figure 2

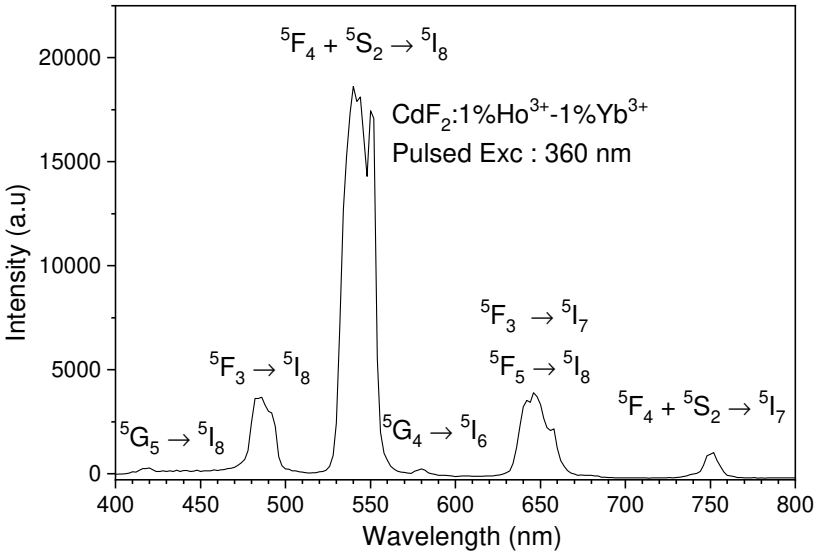
$^5F_4 + {}^5S_2 \rightarrow {}^5I_8$
CdF_2:1%Ho^{3+}-1%Yb^{3+}
Pulsed Exc : 360 nm
$^5F_3 \rightarrow {}^5I_7$
$^5F_5 \rightarrow {}^5I_8$
$^5F_4 + {}^5S_2 \rightarrow {}^5I_7$
$^5F_3 \rightarrow {}^5I_8$
$^5G_5 \rightarrow {}^5I_8$
$^5G_4 \rightarrow {}^5I_6$
Intensity (a.u)
Wavelength (nm)
0
5000
10000
15000
20000
400
450
500
550
600
650
700
750
800

Figure 3

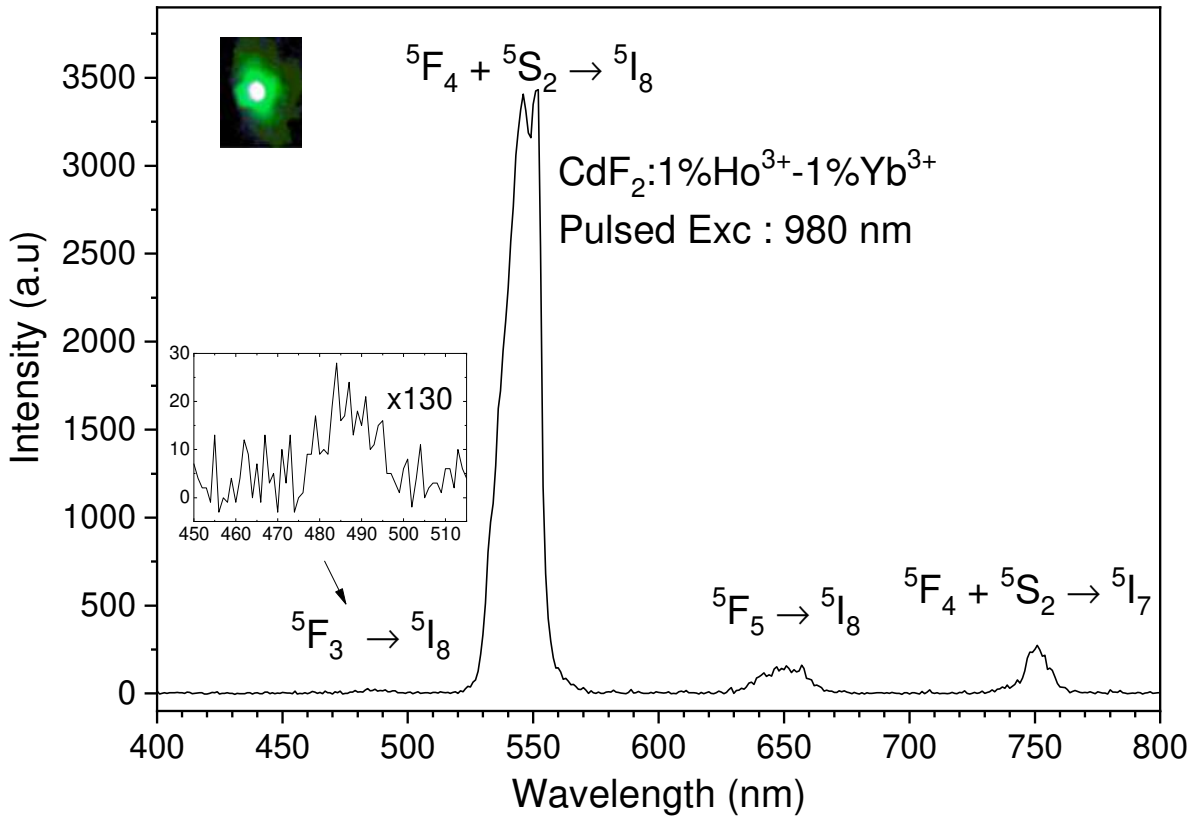
$^5F_4 + {}^5S_2 \rightarrow {}^5I_8$
CdF_2:1%Ho^{3+}-1%Yb^{3+}
Pulsed Exc : 980 nm
x130
$^5F_3 \rightarrow {}^5I_8$
$^5F_5 \rightarrow {}^5I_8$
$^5F_4 + {}^5S_2 \rightarrow {}^5I_7$
Intensity (a.u)
Wavelength (nm)
0
500
1000
1500
2000
2500
3000
3500
400
450
500
550
600
650
700
750
800
30
20
10
0
450
460
470
480
490
500
510

Figure 4

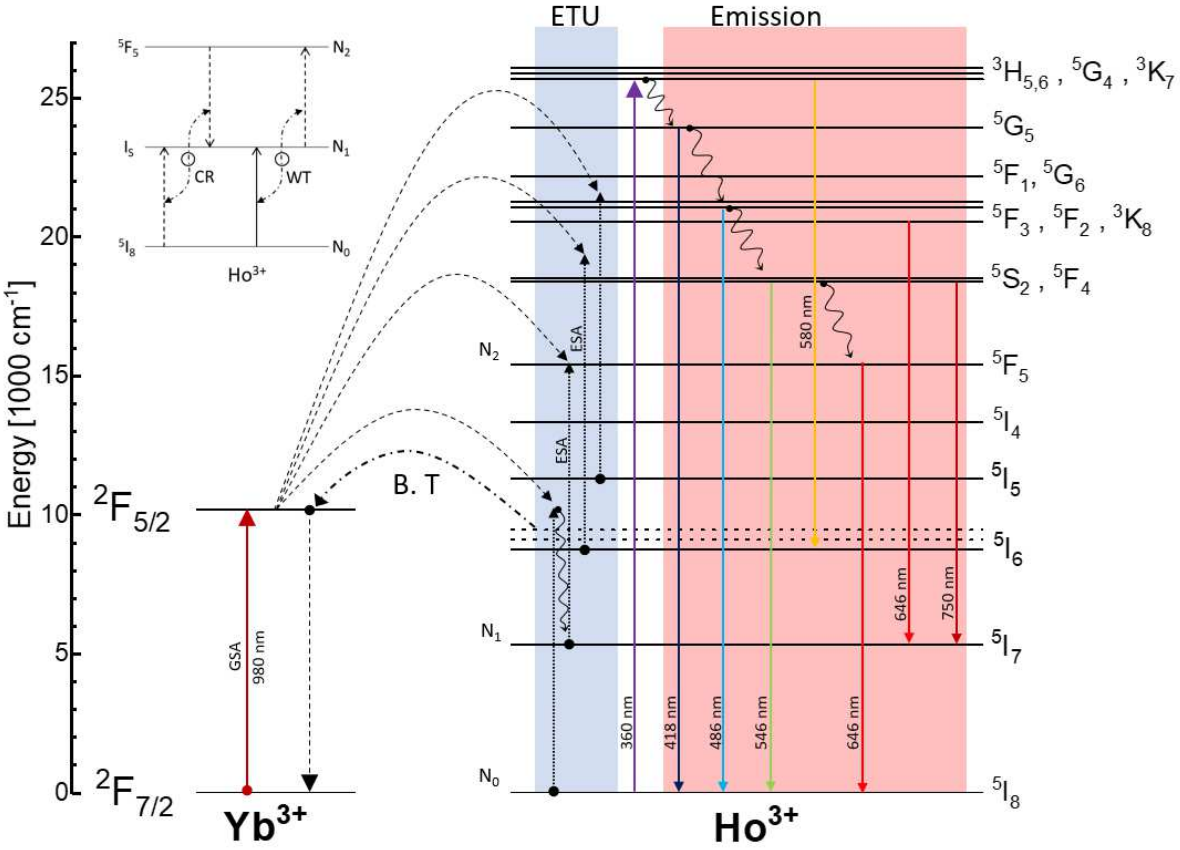
ETU
Emission
Energy [1000 cm-1]
25
20
15
10
5
0
5F5
N2
I5
N1
5I8
N0
CR
WT
Ho3+
2F5/2
2F7/2
GSA
980 nm
B. T
Yb3+
N2
N1
N0
ESA
ESA
360 nm
418 nm
486 nm
546 nm
580 nm
646 nm
646 nm
750 nm
3H5,6 , 5G4 , 3K7
5G5
5F1, 5G6
5F3 , 5F2 , 3K8
5S2 , 5F4
5F5
5I4
5I5
5I6
5I7
5I8
Ho3+

Figure 5

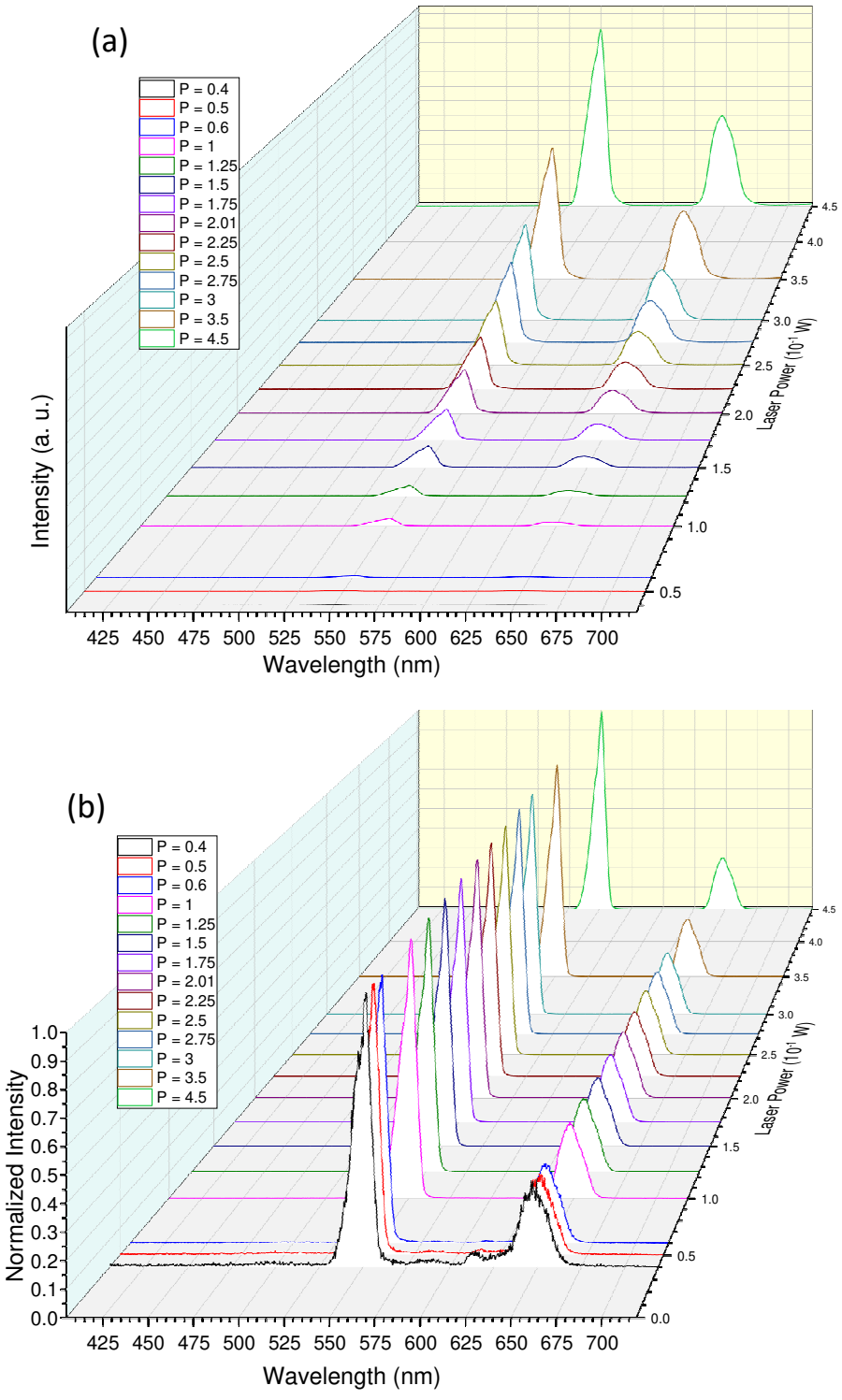
(a)
P = 0.4
P = 0.5
P = 0.6
P = 1
P = 1.25
P = 1.5
P = 1.75
P = 2.01
P = 2.25
P = 2.5
P = 2.75
P = 3
P = 3.5
P = 4.5
Intensity (a. u.)
425 450 475 500 525 550 575 600 625 650 675 700
Wavelength (nm)
0.5 1.0 1.5 2.0 2.5 3.0 3.5 4.0 4.5
Laser Power (10⁻¹ W)
(b)
Normalized Intensity
0.0 0.1 0.2 0.3 0.4 0.5 0.6 0.7 0.8 0.9 1.0

Figure 6

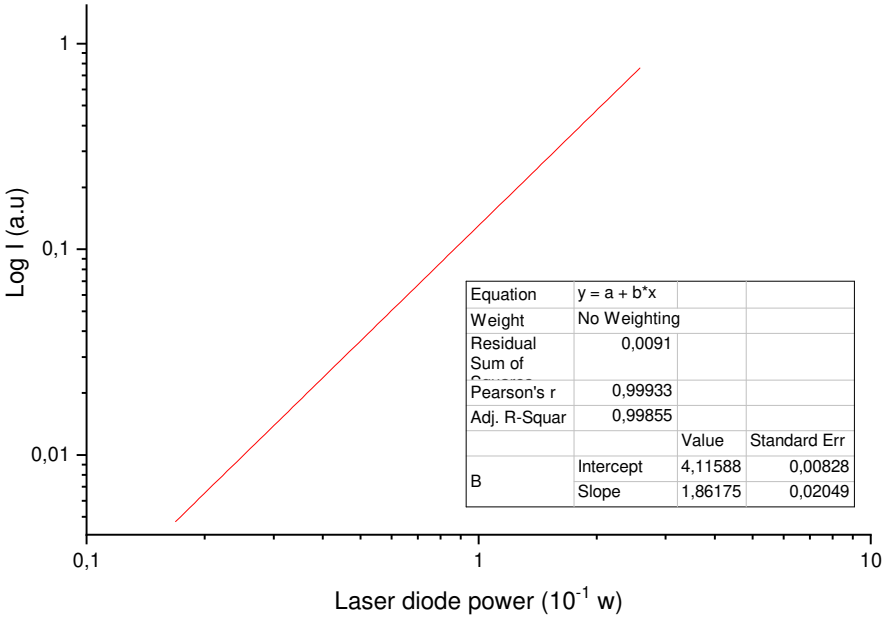
1
0,1
0,01
Log I (a.u)
0,1
1
10
Laser diode power (10^{-1} w)
Equation y = a + b*x
Weight No Weighting
Residual Sum of
Pearson's r 0,99933
Adj. R-Squar 0,99855
Value Standard Err
B Intercept 4,11588 0,00828
Slope 1,86175 0,02049

Figure 7

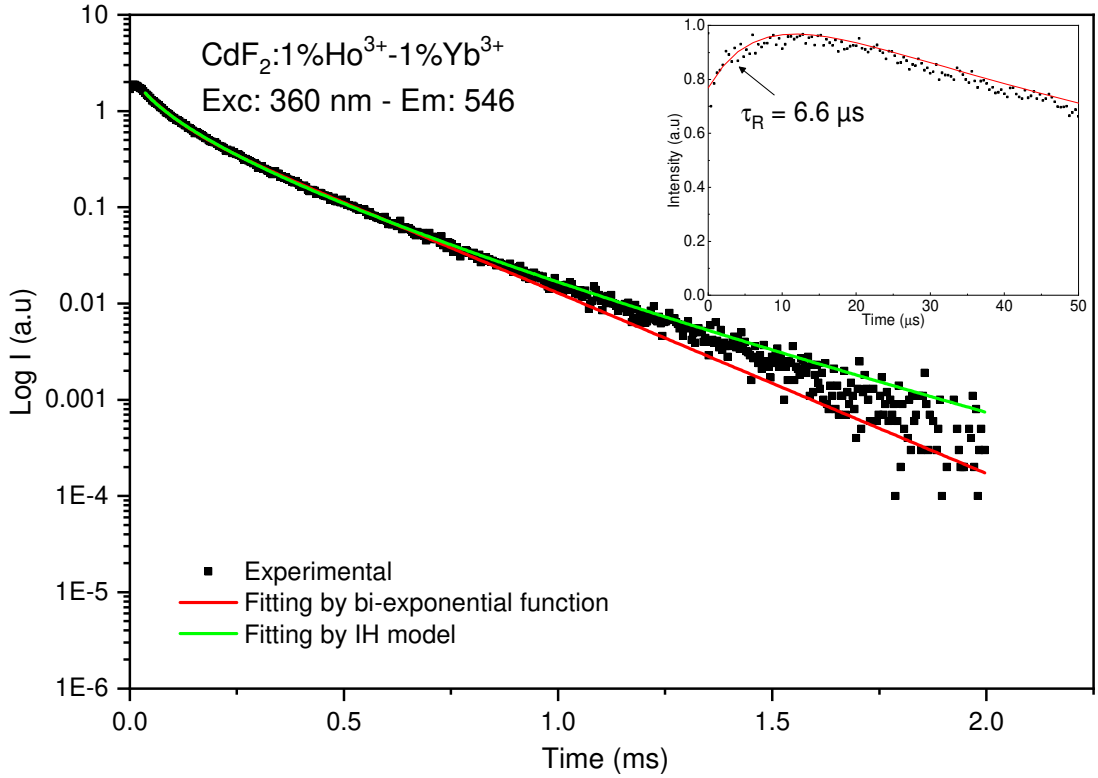
CdF2:1%Ho3+-1%Yb3+
Exc: 360 nm - Em: 546
τR = 6.6 µs
Intensity (a.u)
Time (µs)
Experimental
Fitting by bi-exponential function
Fitting by IH model
Log I (a.u)
Time (ms)

Figure 8

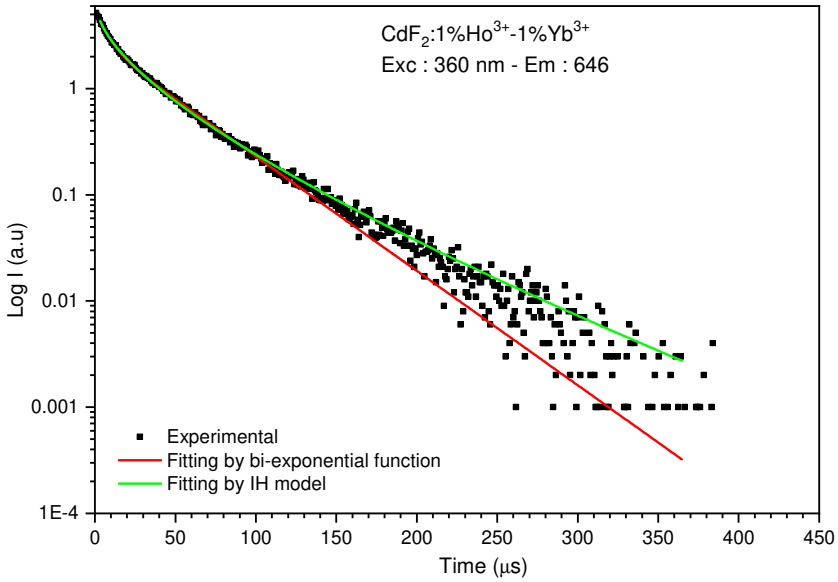
CdF2:1%Ho3+-1%Yb3+
Exc : 360 nm - Em : 646
Log I (a.u)
Time (μs)
Experimental
Fitting by bi-exponential function
Fitting by IH model
1
0.1
0.01
0.001
1E-4
0
50
100
150
200
250
300
350
400
450

Figure 9

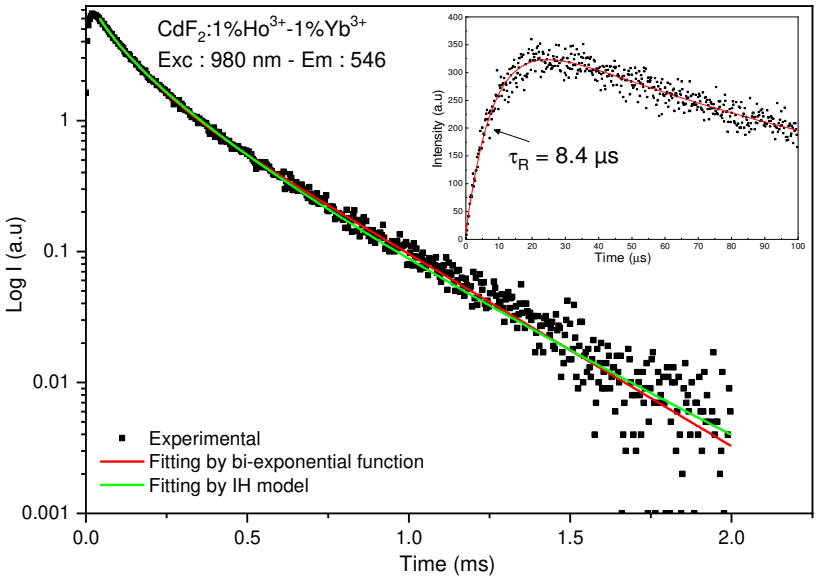
CdF2:1%Ho3+-1%Yb3+
Exc : 980 nm - Em : 546
Log I (a.u)
Time (ms)
Experimental
Fitting by bi-exponential function
Fitting by IH model
Intensity (a.u)
Time (µs)
τR = 8.4 µs

Figure 10

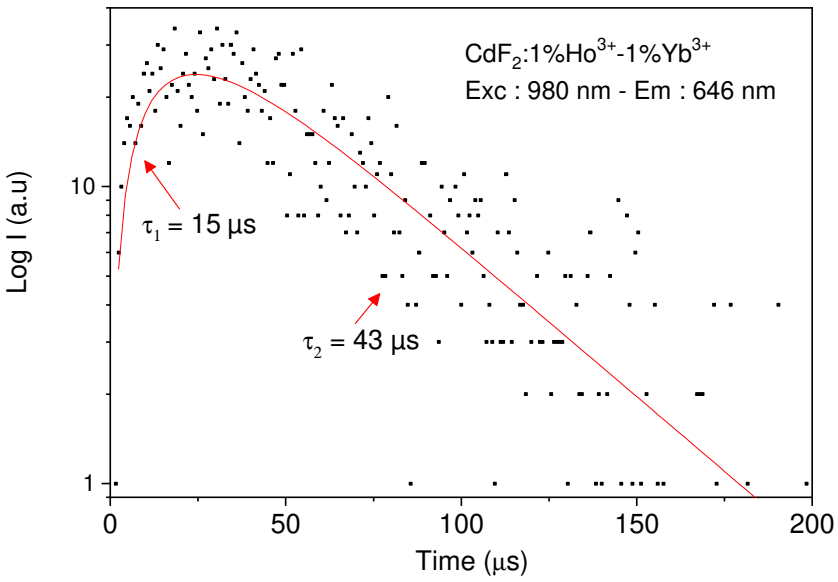
CdF2:1%Ho3+-1%Yb3+
Exc : 980 nm - Em : 646 nm
τ1 = 15 µs
τ2 = 43 µs
Log I (a.u)
10
1
0
50
100
150
200
Time (µs)

Table

Table 1: Experimental values of time constants (μs) derived from fitting by sum of exponential functions of the luminescence decays for green and red emissions of Ho^{3+} in CdF_2 under UV and NIR excitations.

Emission (Excitation)	τ_R	τ_1	τ_2	τ_{Av}
546 nm (360 nm)	6.6	67	250	202
646 nm (360 nm)	-	47	103	85
546 nm (980 nm)	8.4	97	296	219
646 nm (980 nm)	15	43	-	-

Table

Table 2: Experimental values of τ_0, C_A/C_0, critical concentration (C_0), energy transfer microparameter (C_{DA}), and critical distance (R_0) derived from fitting by I-H model for both green and red emissions of Ho^{3+} in CdF_2.

Emission (Excitation)	τ_0 (μs)	C_A/C_0	C_A (10^{20} ions/cm^3)	C_0 (10^{20} ions/cm^3)	C_{DA} (10^{-39} cm^{6}s^{-1})	R_0 (Å)
546 nm (360 nm)	631	1.7	5.1	3	1.1	9.3
646 nm (360 nm)	125	1.64	5.1	3.1	4.9	9.2
546 nm (980 nm)	590	1.36	2.55	1.9	2.8	10.8

Graphical Abstract